Secondary Aerosol Formation in Incense Burning Particles by Ozonolysis and Photochemical Oxidation via Single Particle Mixing State Analysis

Zhancong Liang[1,2], Liyuan Zhou[1,2], Xinyue Li[1], Rosemarie Ann Infante Cuevas[1,2], Rongzhi Tang[1,2], Mei Li[3,4], Chunlei Cheng[3,4], Yangxi Chu[5], Patrick. K.H. Lee[1], Alvin. C.K. Lai[1], Chak K. Chan[1,2,6]*

[1] School of Energy and Environment, City University of Hong Kong, Hong Kong, China
[2] City University of Hong Kong Shenzhen Research Institute, Shenzhen, China
[3] Institute of Mass Spectrometry and Atmospheric Environment, Guangdong Provincial Engineering Research Center for On-line Source Apportionment System of Air Pollution, Jinan University, Guangzhou 510632, China
[4] Guangdong-Hongkong-Macau Joint Laboratory of Collaborative Innovation for Environmental Quality, Guangzhou 510632, China
[5] State Key Laboratory of Environmental Criteria and Risk Assessment, Chinese Research Academy of Environmental Sciences, Beijing, 100012, China
[6] Low-Carbon and Climate Impact Research Centre, City University of Hong Kong, Hong Kong, China

Correspondence to: Chak K. Chan (*chak.k.chan@cityu.edu.hk*)

Abstract. Incense burning is a common religious activity that emits abundant gaseous and particulate pollutants into the atmosphere. During their atmospheric lifetime, these gases and particles are subjected to oxidation, leading to the formation of secondary pollutants. We examined the oxidation of incense burning plumes under O_3 exposure and dark condition using an oxidation flow reactor connected to a single particle aerosol mass spectrometer (SPAMS). Nitrate formation was observed in incense burning particles, mainly attributable to the ozonolysis of nitrogen-containing organic compounds. With UV on, nitrate formation was significantly enhanced, likely due to HNO_3/HNO_2/NOx uptake triggered by OH chemistry, which is more effective than ozone oxidation. The extent of nitrate formation is insensitive to O_3 and OH exposure, which can be explained by the diffusion limitation on interfacial uptake. The O_3-UV-aged particles are more oxygenated and functionalized than O_3-Dark-aged particles. Oxalate and malonate, two typical secondary organic aerosols (SOA), were found in O_3-UV-aged particles. Our work reveals that nitrate, accompanied by SOA, can rapidly form in incense-burning particles upon photochemical oxidation in the atmosphere, which could deepen our understanding of air pollution caused by religious activities.

1 Introduction

Incense burning is a common religious ritual, especially in Asian and African communities (Ye et al., 2016; Khezri et al., 2015; Sidibe et al., 2022), with a massive amount of particles emitted (Lyu et al., 2021; See et al., 2011). The $PM_{2.5}$ concentration at a shrine area reached 6-8 times higher than usual during the Chinese New Year in Chiang Mai, Thailand, mainly due to incense burning (Bootdee et al., 2016). The particle emission factor (i.e., the mass ratio of the emitted particles

to the total material burnt) from incense burning could be up to 10 times higher than those from burning of various types of biomasses such as rice straw (Akagi et al., 2011; See et al., 2011; Goel et al., 2020).

Previous research mainly focused on the chemical compositions and potential health impacts of fresh incense particles (Li et al., 2012; Wang et al., 2006; Chuang et al., 2011; Lee et al., 2004). However, it was rarely considered that fresh particles would also be exposed to other atmospheric pollutants and light, which could initiate chemical reactions. The formation of secondary particulate pollutants could take place during the atmospheric aging of particles (Hodshire et al., 2019; Kumar et al., 2018; Rudich et al., 2007). For example, our recent work reveals rapid sulfate formation in fresh incense burning particles upon SO_2 exposure in the dark, and it can be accelerated under light (Liang et al., 2022). Sulfate formation in incense burning particles under dark and light was mainly attributed to gaseous oxidants and particulate photosensitizers, respectively.

Ozone and OH radicals are two of the most common oxidants in the atmosphere, contributing to secondary inorganic and organic aerosol formation (Volkamer et al., 2006; Kroll et al., 2006; Chen et al., 2011; Liu et al., 2019; Liu et al., 2018). Incense burning plume has been reported to contain various volatile organic compounds (VOCs) and NOx (Lee et al., 2004; Ho et al., 2002), in addition to particulate pollutants. Their interactions with ozone and OH radicals may lead to secondary aerosol formation. For instance, ozone and OH oxidations of NOx were considered primary sources of particulate nitrate (Seinfeld et al., 2008; Liang et al., 2021; Gen et al., 2022). Nevertheless, there is still a lack of understanding of the secondary aerosol formation in incense burning particles upon atmospheric aging of the plume, which could potentially worsen air quality, especially near areas of intense religious activities.

This study examines the secondary aerosol formation in fresh incense burning particles under ozone and OH exposure using a Gothenburg Potential Aerosol Mass (Go: PAM) flow reactor. We first characterized single fresh incense burning particles, followed by aged particles, with a single-particle aerosol mass spectrometer (SPAMS). Control experiments were performed to get insight into the possible secondary aerosol formation pathways and their significance. Then, we discussed nitrate formation as a function of particle size, ozone, and OH exposure. The fragmentation severely hinders the characterization of secondary organic aerosol (SOA). Nevertheless, -89[C_2HO_4] (oxalate) and -103[$C_3H_3O_4$] (malonate), two commonly considered SOA(Cheng et al., 2017; Sullivan et al., 2007), were found.

2 Experimental

2.1 Aging of incense-burning particles

The schematic of the experimental set-up can be found in Figure S1. In brief, we burnt an incense stick (Figure S2, Kwok Tin Heung, Hong Kong) in a 20 L glass burning bottle for each experiment. The air exchange rate per hour (ACH) is 0.3, comparable to the typical natural ventilation conditions (Lee et al., 2004). The relative humidity (RH) and the temperature inside the burning bottle were 56 ± 9 % RH and 22 ± 2.7 °C. The burning was rapidly converted from flaming to smoldering

after ignition. A two-stage system diluted the emissions with an overall dilution of around 1600. Compressed air (~0.1 L min^{-1}) was used to introduce the diluted incense burning particles to the PAM reactor equipped with two UVC light tubes (30W, Philips TUV, λmax = 254nm). The spectrum of the lamp was shown in Supplementary information (Figure S3). In the control experiments, a charcoal absorber or HEPA filter was used to remove the gaseous pollutants or particles prior to the introduction to the Go:PAM. The data of these control experiments can be found in the supplementary information (Figure S4, S5). All these control experiments were aged experiments. The removal efficiency of NOx, VOCs, and particles were ~85%, ~90%, and ~100%, respectively, determined by the concentration reduction after applying a HEPA filter or charcoal absorber at the exhaust of the burning bottle, using a NOx analyzer (T200, Teledyne) or a Total VOC analyzer (Yuante) (Figure S1). A controlled dry-wet mixed carrier flow of compressed air (~4 L min^{-1}) and a flow of O_3 (~0.1 L min^{-1}) generated by passing O_2 (99.995%, Linde) to an O_3 generator (Model 610, Jelight Company Inc, USA) were introduced into the Go:PAM. The compressed air was treated by a HEPA filter and a charcoal absorber prior to the experiment system. [O_3] ranged from 300 to 1500 ppb, equivalent to an atmospheric ozone exposure of 10-50 min, assuming ambient concentration of 60 ppb (Xia et al., 2021). The RH at the exit of the PAM was monitored by an RH sensor (M170, Vaisala, Finland). All the experiments were conducted at 80% RH and 22 ± 1.7 °C. The residence time in the Go:PAM was ~100 s. The exhaust of the PAM was characterized by an O_3 analyzer (106L, 2B technology, USA), a water-based condensation particle counter (WCPC, Aerosol dynamics Inc, USA), and a SPAMS (Hexin Analytical Instrument Co., Ltd, China). Watne et al. suggested that the penetration of the particles is close to 100% for particles larger than 100 nm. Hence the wall loss is negligible for the 0.2-2 um particles that SPAMS measures. Besides, a control experiment measuring the total VOCs at the entrance and the exhaust of the Go:PAM suggested that the gas wall loss was also minor (6 ± 4%). The particles passed through a diffusion dryer before entering the Go:PAM to reduce the matrix effects from water (Neubauer et al., 1998). The RH at the exhaust of the diffusion dryer was ~15%. The residence time of the particles in the dryer was estimated to be 5 s and the particle loss was ~4% according to the CPC measurements. We also collected particles on 47 mm quartz filters (PALL, USA) at the exhaust of the Go:PAM reactor for offline mass and chemical analysis. The number of particles collected on the filters was estimated by the total WCPC counts during the sampling period. The particle number concentration from the WCPC was 6100 ± 2400 # cm^{-3} and the estimated number of collected particles was around 10^8 #. The filter sample was extracted by deionized (DI) water for analyzing water-soluble ions (e.g., nitrate, formate, potassium) by Ion chromatography (IC) using the same protocol reported in our previous work (Liang et al., 2022). The total organic content (TOC) of the water-extract was analyzed by a TOC analyzer (Shimadzu TOC-L).

We studied the aging of the particles under 'UV', 'O_3 and dark', and 'O_3 and UV' in the PAM. We named these aged particles UV-aged, O_3-Dark-aged, and O_3-UV-aged, respectively. Although 254 nm is not atmospherically relevant, UV-aged particles are used as a reference in the discussions of the properties of O_3-UV-aged particles. The OH exposure, equivalent to the product of gas-phase OH concentration and residence time, was determined by introducing a stream of SO_2 to the PAM for consuming OH radicals and monitoring the [SO_2] decay, following a well-established approach in the literature (Kang et al., 2007). [SO_2]

was almost constant under UV on but without O_3, suggesting that the photochemistry of incense plume does not affect our estimation of OH exposure. The upper limit of OH exposure used in this study varied from 1×10^{10} to 5×10^{10} molecules cm^{-3} s, equivalent to 2~10 hours of photochemical aging, assuming an ambient OH concentration of 1.5×10^6 molecules cm^{-3} (Mao et al., 2009).

2.2 SPAMS analysis

A detailed description of the SPAMS can be found in Li et al (Li et al., 2011). After the particle flow exits the PAM reactor, it first passes a $PM_{2.5}$ cyclone to avoid clogging before entering the SPAMS through a 0.1 mm critical orifice at 80 mL min^{-1} flow. Particles achieved a terminal velocity in the supersonic expansion airflow and were detected and aerodynamically sized by two continuous diode Nd: YAG laser beams (532 nm). They were then ionized by a pulsed Nd: YAG laser (266 nm) triggered based on the velocity of a specific particle. The positive and negative ions produced were detected according to the different mass-to-charge ratios (m/z). The energy of the ionization laser was kept at ~0.6 mJ (Cheng et al., 2017). Spectra of more than 3000 individual particles collected for ~15 min were used for further analysis for each experiment. The size accuracy of the instrument was routinely calibrated with polystyrene latex spheres of 0.2-2.5 μm diameter (Nanosphere Size Standards, Duke Scientific Corp., Palo Alto). An adaptive resonance theory method (ART-2a) based on MATLAB was used to categorize the incense particles of similar SPAMS spectral characteristics into different particle groups (Phares et al., 2001). In the ART-2a analysis, we used a vigilance factor of 0.85, and more than 98% of the particles were classified. Note that there is no general rule for the vigilance factor in ART-2a. Zhao et al. (2008) reported that both a small vigilance factor (e.g., 0.5 or 0.6) and a relatively high vigilance factor (e.g., 0.8) show very similar clustering accuracies (± ~5%) (Zhao et al., 2008).

3 Results and discussions

3.1 Single-particle characteristics of incense burning particles

The relative peak area (RPA), defined as the peak area of a specific peak divided by the total positive or negative mass spectral peak area, can reflect the relative abundance of particulate components (Liang et al., 2022). Note that RPA is not equivalent to concentration due to the matrix effect. Furthermore, control experiments using different laser fluences indicate that partial ablation was insignificant (Table S1, will be discussed later). The average spectra of the incense burning particles (Figure 1a) are similar to our previous work on incense burning at 50% RH (Liang et al., 2022). +39[K] dominates the positive spectra, and organic nitrogen (ON) peaks (i.e., -26[CN] and -42[CNO]) from nitrogen-containing organics (NOC) dominate the negative spectra (Zhang et al., 2020; Zhai et al., 2015; Zhang et al., 2021). These features are also found in biomass burning particles (Bi et al., 2011; Peng et al., 2019; Luo et al., 2020). Despite that particulate polyaromatic hydrocarbons (PAHs) were found in a previous incense combustion study (Ji et al., 2010) and a recent study of ambient particles based on a single-particle mass spectrometer with ART-2a (Passig et al., 2022), none of the fresh incense burning particles in our experiments contained

the PAHs peaks (m/z = 178, 189 (fragment of alkylated phenanthrenes), 202, 220, 228, and 252). Regardless of the presence of PAHs or not, our conclusion on nitrate formation does not depend on the detection of specific chemicals such as PAHs.

ART-2a categorizes fresh incense burning particles into K-ON, K-ONEC, K-Cl, and OC-ON. EC, Cl and OC are abbreviations of elemental carbon, chloride and organic carbon, respectively. Briefly, the "K" and "OC" before the hyphen indicate the characteristics of the positive spectra, while "ON", "ONEC" and "Cl" after the hyphen indicate the characteristics of the negative spectra. "K-" particles contain a dominant +39 peak and a small +41 peak attributed to isotopic potassium (Silva et al., 1999). On the other hand, the "OC-" particles are rich in typical organic fragments such as +27[C_2H_3] (Silva et al., 2000). According to the negative spectra, "-ON" particles have dominant ON signals. "-ONEC" particles have elemental carbon (EC) peaks of -12n[C_n^-], with intensities comparable to typical ON peaks (Whiteaker et al., 2002). "-Cl" particles have prominent Cl^- (m/z=-35, -37(isotopic)) and KCl_2^- (m/z=-109, -111(isotopic)) peaks (Guazzotti et al., 2001; Dall'osto et al., 2004). The average spectra of each category can be found in Figure S6. There are slightly fewer K-ON particles and more K-ONEC particles observed at 80% RH (this work) than at 50% RH in Liang et al (Liang et al., 2022), probably due to the lower organic concentrations at higher RH to limit particle-phase partitioning of volatile organic compounds (Donaldson et al., 2006; Mcfall et al., 2020; Chan et al., 2011; Chan et al., 2010). Overall, the number fraction (NF) of each category is similar to our previous work, with a descending order of K-ON (47.3±5.2%) >> OC-ON (25.7±4.7%) ≈ K-ONEC (20.2±2.8%) > K-Cl (5.1±1.1%) (Figure 1c), reflecting the fresh incense burning particles are organic-rich (Li et al., 2012; Zhang et al., 2022).

3.2 Ozonolysis of the incense burning particles

Figure 1a also shows the average spectra of aged incense burning particles under 800 ppb O_3. Qualitatively, the major peaks are similar to those in fresh incense burning particles, except for the rise of -62[NO_3^-] and -46[NO_2^-], which indicates the formation of nitrate and probably nitrite. The formation of organo-nitrate is not considered significant due to the decreased -26[CN] and -42[CNO].

To compare the changes in the organic signals, we first excluded all inorganics and EC peaks (Table S2). Control experiments atomizing KNO_3 solution (as K^+ is the main inorganic cation found in incense burning particles) showed the RPA ratio of -16[O] to nitrate peaks is (6 ± 1.7) % due to fragmentation. Sulfate shows negligible fragmentation under our experimental conditions (Liang et al., 2022). Thus, we subtracted the RPA of -16[O] by 6% RPA of nitrate. Then, we recalculated the RPA of the organic peaks only, defined as “organic spectra”. Figure 1b shows the differences in the organic spectra of the aged and fresh particles. The positive difference spectra show an RPA increase in the hydrocarbon +37[C_3H] but an RPA decrease in +51[C_4H_3](Dall'osto et al., 2013). Besides, the increase of +28[CO], +42[C_2H_2O], and +43[C_2H_3O] indicates the formation of oxidized organics in the particles during ozonolysis. The negative difference spectra show a decrease in ON peaks, possibly due to the destruction of C-N bonds under ozonolysis, and an increase of -45[CHO_2] formate peak.

NO_2 emitted by incense burning may hydrolyze in the incense burning particles to form nitrite and nitrate ($2NO_2 + H_2O \Rightarrow HNO_2 + HNO_3$) (Finlayson-Pitts et al., 2003; Ramazan et al., 2006). The uptake of NO_2 is slow in deionized water ($\gamma \approx 10^{-7}$), but it could be significantly promoted by chloride ($\gamma \approx 10^{-3}$ in 1mM NaCl) (Enami et al., 2009; Yabushita et al., 2009), which is found as major inorganic anion in the incense burning particles. In addition, the reaction between NO_2 and O_3 produces NO_3 radicals, which could react with organics to form organo-nitrate (Ng et al., 2017). However, control experiments using a charcoal absorber to remove NOx only show ~20% decrease in RPA of total nitrate in O_3 aged particles (Figure S4), indicating that NO_2 hydrolysis and nitration may not be the main contributor to the nitrate formation. The charcoal absorber removes both NOx and VOC. However, it was not expected to be important in the observed nitrate RPA reduction, as the content of nitrogen-containing VOCs was minor in the incense burning plume, according to the literature (Manoukian et al., 2013). We categorized the O_3-Dark-aged particles into 7 groups of K-ON, K-ONEC, K-ONN, K-N, K-Cl, OC-N, and OC-ON particles by ART-2a. The definitions of K-, OC-, -ON, -ONEC, -Cl are the same as before. -N particles show prominent nitrate peaks (-46[NO_2] and -62[NO_3]) in the negative spectra, while -ONN particles show comparable ON peaks and nitrate peaks (Figure S6). The NF of different categories descends in the order of K-ON (29.0±0.7%) ≈ K-ONEC (22.8±1.8%) ≈ OC-N (21.9±1.0%) > K-ONN (11.2±0.9%) > OC-ON (7.6±1.7%) > K-Cl (3.9±0.4%) > K-N (2.5±0.5%) (Figure 1c). Interestingly, the K-ONEC and K-Cl NFs are similar before and after aging, whereas the K-ON NF decreased, and the decrease is comparable to the sum of the K-ONN and K-N NF increases. OC-ON was the only fresh OC- particle type, but OC-N was dominant after aging. A control experiment with a HEPA filter before the Go:PAM showed no detectable particles by SPAMS. Thus, we assume the total SPAMS-detectable particle number was constant before and after aging, and O_3-aging may have preferentially converted some -ON type particles to nitrate-containing particles (i.e., -ONN, -N). It has been reported that the HEPA filter would cause the loss of semi-volatile VOC (SVOC) or less-volatile VOC (LVOC) (Schilling, 1997). However, the addition of the charcoal to remove VOCs at the exhaust only caused ~6 % reduction of the NF of -ON type particles and nitrate-containing particles (i.e., -ONN, -N), suggesting the roles of SVOC and LVOC were minor to our conclusion. Besides, O_3-Dark-aged particles have lower ON (i.e., the sum of -26[CN] and -42[CNO]) absolute peak area (APA) and higher total nitrate APA (i.e., -46[NO_2] and -62[NO_3]), than fresh particles (Figure S7). We considered -46[NO_2] mainly as a nitrate fragment but not nitrite since the IC-measured [NO_2^-]/[NO_3^-] in the water-extract of collected particles was very low (~0.01) (Figure S8). We used APA here because it reflects the total abundance of ions and would not affect the analysis of other ions (Spencer et al., 2006). The formation of nitrate would increase the total peak area and decrease the RPA of other peaks, even the APA of others kept constant. Figure S9 also shows a positive correlation between the total nitrate RPA and formate RPA in the aged particles. Based on offline IC analysis, the water-extract of O_3-Dark-aged particles has higher [Formate]/[K^+] and [NO_3^-]/[K^+] in than fresh particles (Figure S10), assuming that K^+ is not reactive and used as an internal standard (Figure S11). Taking these altogether, nitrate and formate likely formed together, preferentially on K-ON and OC-ON particles. Ozonolysis of NOC has been reported to generate nitrate and formate (Sharma et al., 2010; Yao et al., 2020).

3.3 Photochemical oxidation of incense burning particles

With UV (254nm) on, the 800 ppb O_3 was partly photolyzed to generate OH radicals in the presence of water vapor, resulting in an OH exposure of ~3× 10^{10} molecules cm^{-3} s, equivalent to a photochemical age of ~5 h. We will use xx ppb O_3 (initial concentration) +UV, instead of OH exposure, to describe OH aging. The average spectra of O_3-UV-aged particles are generally similar to that of O_3-Dark-aged particles, with potassium and nitrate peaks dominating the positive and negative spectra, respectively (Figure 1a). However, the RPA of -46[NO_2] and -62[NO_3] were 0.2 and 0.4, around 2 times higher than O_3-Dark-aged particles, likely indicating more nitrate formation. As will be discussed later, photochemistry triggered by light-absorbing compounds such as photosensitizers and Fe salts is a possible source of nitrate formation in O_3-UV-aged particles.[51-53] However, its contribution is considered minor compared with OH chemistry since UV-aged particles only show a total nitrate RPA of 0.05, much lower than that of O_3-UV-aged particles (~ 0.7, will be discussed later). Control experiments using a charcoal absorber to remove the NOx significantly reduced the RPA of total nitrate by ~75% (Figure S4). These suggest that OH chemistry involving NOx dominated the particulate nitrate formation under OH exposure. Under 800 ppb O_3 and UV, the ~90% reduction of [NOx] with a simultaneous increase in total nitrate peaks under UV suggests the oxidation of NOx by OH radicals to form HNO_2 and HNO_3, which can be uptake by the particles afterward (Finlayson-Pitts et al., 1999). Reactive uptake of NOx initiated by OH chemistry cannot be excluded.

Similar to the O_3-Dark-aged particles, O_3-UV-aged particles show decreases in ON and other organic peaks (+38[C_3H_2], +50[C_4H_2], and +51[C_4H_3]) in the difference organic averaged spectra (Silva et al., 2000), likely due to oxidative consumption by OH radicals (Figure 1b). The ON peaks decrease in O_3-UV-aged particles was more significant than in O_3-Dark-aged particles, whereas the increase in formate peak is less obvious. These indicate that NOCs can also be effectively degraded via OH oxidation. Using the commonly used general markers of oxidized/aged organics in single-particle mass spectrometric studies of -16[O], -17[OH], +42[C_2H_2O], and +43[C_2H_3O] as examples (Taiwo et al., 2014; Denkenberger et al., 2007; Qin et al., 2006), the RPA increase in O_3-UV-aged particles are 18, 10, 3, and 17 times higher than in O_3-Dark-aged particles. This suggests that OH aging produced more oxidized products than O_3 aging. The difference average organic spectra of UV-aged particles almost showed no noticeable peaks, indicating that the chemistry initiated by particulate photoactive compounds may not be essential to the transformation of the organics (Figure S12).

The O_3-UV-aged particles can be categorized into K-ONN, K-N, and OC-N, and they generally have more intense nitrate peaks than O_3-Dark-aged particles. Still, "-ONN" particles have comparable ON and nitrate peaks, and "-N" particles have dominant nitrate peaks in the negative spectra (Figure S6). The NF descends in the order of OC-N (35.7±7.2%) ≈ K-N (35.5±4.2%) > K-ONN (25.7±2.1%) (Figure 1c). Notably, the NF of OC- particles of O_3-UV-aged particles is 50% larger than the fresh particles, likely due to the formation of additional particulate organics. We could not identify any preferential nitrate formation in specific particle types since most of the particles have high RPA of nitrate. The collection efficiency of SPAMS

increased from ~1% at 200 nm to ~40% at 960 nm (Figure S13). Therefore, secondary aerosol formation in small particles may have been underestimated. However, this would not affect the conclusion of the results that nitrate formed in incense burning particles upon O_3+Dark and O_3+UV aging. A control experiment doubling the laser fluence from 0.6 to 1.2 mJ showed minor differences in the classification of the aged particles and the RPA of total nitrate peaks (Table S1). This suggested that the partial ablation due to the formation of nitrate coating is not significant. It is possible that there were some pure secondary organic particles still not ionized at 1.2 mJ, which resulted in an underestimation of secondary organic aerosol formation.

3.4 The formation of secondary nitrate

Figure 2a shows the RPA of nitrate peaks under UV and different exposure of O_3 and OH. Since fresh particles also have high NF of total nitrate, NF cannot accurately depict the effectiveness of nitrate formation. Fresh incense burning particles exhibit very low RPA of total nitrate, whereas exposure to O_3 increases the RPA from almost 0 to around 0.2, irrespective of the [O_3]. Only a slight increase (~0.02) in total nitrate RPA was observed for UV-aged particles. However, with both O_3 and UV on, the RPAs of total nitrate further increased to above 0.7, which is also independent of the initial [O_3]. Consistent with the average spectra shown before, nitrate formation due to OH oxidation is likely more efficient than that by ozonolysis. Under both O_3 and OH exposure, the summed APA of nitrate peaks increased as particle size increased, suggesting possibly a larger total amount of nitrate formed in larger particles (Figure 2b, d). However, the RPA shows an opposite trend, which can be interpreted as lower nitrate concentration in larger particles. Larger particles have larger surfaces but smaller surface-to-volume ratios, which lead to a larger absolute amount of nitrate formed but a lower relative concentration of particulate nitrate (Figure 2c, e). It has been reported that the larger organic and inorganic mixed particles could undergo liquid-liquid phase separation (LLPS) more easily than smaller ones (Kucinski et al., 2019). It is possible that the organics are mainly located at the outer layers of the particles, whereas the inorganic components reside in the core. The hydrophobic organic shell may have retarded the uptake of HNO_3/HNO_2/NOx to form nitrate. Under O_3+UV, it is also possible that comparable HNO_3 was generated under excess [OH] and contributed to the similar total nitrate RPA since the [NOx] reductions under different OH exposure are similarly high (Figure S14). The insensitivity of nitrate formation to O_3 and OH exposure can be potentially explained by the diffusion limitation of interfacial uptake due to the poor hygroscopicity of fresh incense burning particles (Li et al., 1993; Zaveri et al., 2018; Slade et al., 2014; Liang et al., 2022).

3.5 The Potential formation of SOA

Oxalate and malonate are two major dicarboxylates in atmospheric particles and are considered SOA (Yao et al., 2002). They have been widely studied using single-particle mass spectrometry with well-validated detection efficiency, without severe complications in mass spectra due to fragmentations (Cheng et al., 2017; Sullivan et al., 2007). Figure 3a shows the NF ratio (aged particles to fresh particles) of oxalate and malonate. We used the NF ratio rather than the APA or RPA to avoid large uncertainties in organic abundance due to the much weaker peaks of organics in the spectra, which was potentially due to the

matrix effects. The APA threshold for oxalate or malonate was 15 arbitrary unit (a.u.) with a baseline of zero unit, the same as that adopted in an ambient study (Zhu et al., 2020).

Compared to 300 ppb O_3 and UV, the NF ratios of malonate and oxalate were 30 and 9 folds higher, at 1500 ppb O_3 and UV, respectively. This trend is different from the independence of nitrate formation on OH exposure, probably because the formation of SOA was slower than nitrate via multiphase uptake. These NFs are lower estimates due to the possible degradation by photolysis of Fe-decarboxylate complexes to CO_2 (Gen et al., 2021). While the TOC ratio at different O_3+UV which indicates the formation of SOA, shows an overall trend similar to the NF ratios of oxalate and malonate (Figure S15), the TOC ratio was 1.2-7.1 folds higher than the NF ratios of oxalate and malonate. However, this could be due to the formation of many other species as well as the matrix effects. SOA formation during aging of incense burning plume should be further assessed by other quantitative online instruments in future work. In contrast, no oxalate and malonate were observed during ozonolysis, irrespective of [O_3]. It is likely the SOA characteristics and precursors are different under O_3 and OH. Hence, we are conservative and use the term "potential", even though oxalate and malonate are commonly found highly oxidized SOA. The TOC ratio of aged to fresh particles extract was higher upon OH oxidation than O_3 oxidation (Figure S16). Furthermore, UV-aged particles did not show an NF increase of both, indicating that the oxalate and malonate formation were mainly due to OH radicals, rather than oxidants from particulate photoactive compounds or ozone. The control experiment with a charcoal absorber shows around 60% and 70% NF reduction of oxalate and malonate, suggesting that the precursors are mainly in the gas phase (Figure S5). The size distribution of oxalate and malonate containing particles skewed towards the larger sizes, supporting their nature of secondary formation (i.e., oxidized gaseous precursors were added to the particles that cause size increase, Figure S17). Figure 3b shows the NF of oxalate and malonate in different categories of the particles. The particles in the replicated experiments under the same OH exposure were combined to compensate for the low particle concentrations. The error bars show one standard deviation among different OH exposures. In descending order, the NF of oxalate and malonate was K-N > K-ONN > OC-N. The mass hygroscopic grow factor (i.e., the mass ratio of wet particles to dry particles) of inorganic potassium salts KNO_3 and KCl at 80% RH are around 1.6 and 2.2 based on AIOMFAC model predictions (Text S1, https://aiomfac.lab.mcgill.ca/about.html (Zuend et al., 2008)), much higher than that in the water extract of biomass burning particles (1.1-1.4, including both lab-generated and ambient collected) (Rissler et al., 2006; Carrico et al., 2008; Chan et al., 2005), as well as fresh incense burning particles (around 1) (Liang et al., 2022), which are organic-rich. The likely higher fraction of hygroscopic inorganic of inorganic fraction allows K-N and K-ONN to retain more liquid water to dissolve gaseous SOA precursors for oxalate and malonate formation. The difference of oxalate and malonate NF is statistically significantly different between K-N and OC-N (i.e., $P < 0.05$ in ANOVA test). There are many other changes in the NF of organic fragments, which suggest the oxidation of primary organics and the formation of SOA. However, further analysis was limited by the lack of molecular information after severe fragmentation. The major spectral evolution and possible peak attribution can be found in Text S2.

4 Conclusions

In this work, we report the single-particle mixing state characteristics of incense burning particles upon ozonolysis and photochemical oxidation. Formation of secondary aerosol including nitrate and organics was found. This indicates that besides the significant primary emission of particles, additional particulate pollutants could be formed upon atmospheric aging, further worsening the air quality in both outdoor and indoor environments. Nitrate formation initiated by O_3 is generally considered to involve the so-called N_2O_5 pathway, in which oxidation of NOx forms NO_3 radical and then N_2O_5, which hydrolyzes to form particulate nitrate (Zhao et al., 2021; Xiao et al., 2020). In our study, nitrate formation was found, as indicated by the increase of total nitrate RPA from near 0 to around 0.2, upon O_3 exposure. We propose that ozonolysis of NOCs may be a potential pathway for nitrate formation, in addition to the N_2O_5 pathway. With UV on, ozone was photolyzed to form OH radicals, and we observed a significant increase in total nitrate RPA to above 0.7 at 300 ppb O_3 or above. Nitrate formation in O_3-UV-aged particles is more prominent than in O_3-Dark-aged particles and is attributed to multiphase OH oxidation involving NOx, such as HNO_3/HNO_2/NOx uptake (Chen et al., 2020; Lu et al., 2019). At 300 ppb O_3 and UV in this study, the equivalent OH and O_3 exposure time of the incense particles is estimated to be ~2 h and ~10 min, respectively, assuming daytime OH and O_3 concentration of 1.5×10^6 molecules cm^{-3} and 60 ppb (Xia et al., 2021; Mao et al., 2009). Despite the differences in the estimated exposure time for OH and O_3, nitrate formation in incense particles under sunlight can be efficient.

We also observed various changes in organics peaks, though less apparent than nitrate in the average spectra. Overall, oxygenated fragments like +42[C_2H_2O] increase, which indicates functionalization of the organics upon oxidation. The increase of such oxygenated fragments is more significant in O_3-UV-aged than O_3-Dark-aged particles. -26[CN] and -42[CNO] attributed to NOC decreased under O_3 and OH exposure. Apparent formate formation was observed in O_3-Dark-aged particles, likely from the degradation of NOC. Production of formate in O_3-UV-aged particles was less significant than that in O_3-Dark-aged particles, attributed to the photolysis of O_3. Oxalate and malonate were observed in O_3-UV-aged particles but not in O_3-Dark-aged particles, and the NFs increased with OH exposure. Furthermore, oxalate and malonate preferentially formed on K-N particles, followed by K-ONN and then OC-N, indicating a potentially crucial role of aerosol liquid water in SOA formation.

Though the molecular characterization of SOA is beyond the focus of this work, the formation of oxalate and malonate shed light on the SOA formation upon photochemical oxidation of the incense burning plumes. Formate and dicarboxylates are important hygroscopic organics in atmospheric particles, which can potentially act as cloud condensation nuclei (Yao et al., 2002; Peng et al., 2001). Incense burning particles were often used as biomass burning particle surrogates (Li et al., 2012; Schurman et al., 2017; Zhang et al., 2014; Kuwata et al., 2017), due to their similar physicochemical properties and overall composition (Li et al., 2012; Zhang et al., 2022). Our work sheds light on the secondary aerosol formation in biomass burning particles upon exposure of atmospheric oxidants, despite that the detailed composition of incense burning plume may be different from biomass burning plume because of the manufacturing process of incense sticks. For instance, incense burning

sticks may contain additives such as adhesives beyond biomass constituents (Lin et al., 2007). Future works are encouraged to explore the formation mechanism and kinetics of secondary pollutants in the incense burning and biomass burning particles. Due to the short residence time in a PAM reactor, assumption in the interchangeability of oxidant concentration and reaction time in estimating total exposure was made. However, Chu et al. (2019) challenged such interchangeability in ozonolysis reaction of linoleic acid (Chu et al., 2019). Aging at ambient concentrations of oxidants should also be investigated.

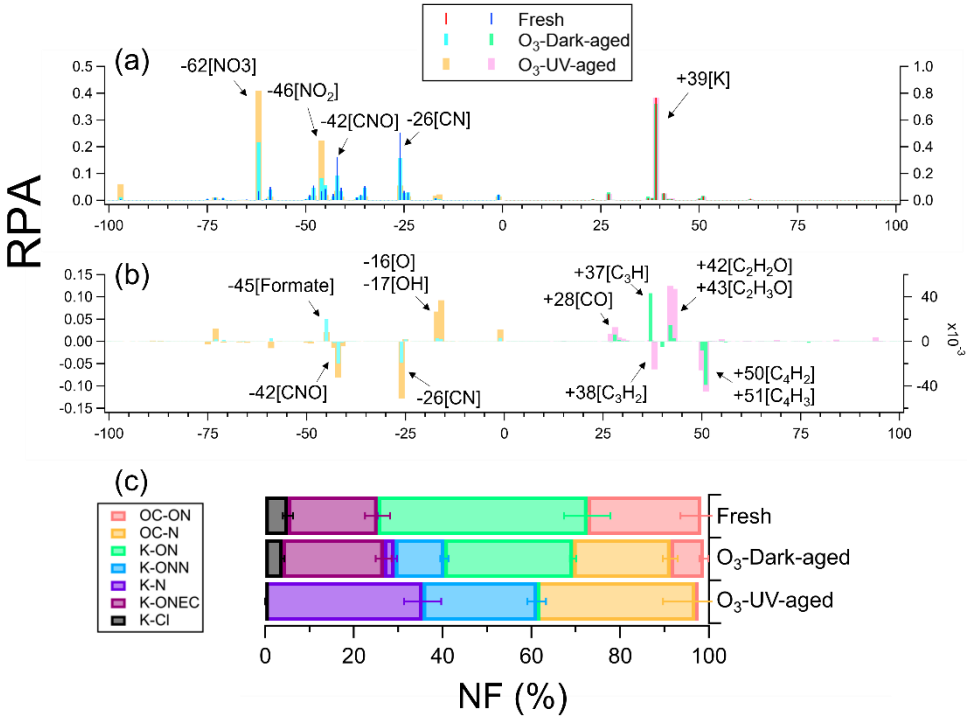

Figure 1. (a) The average spectra of fresh and aged incense burning particles at 800 ppb O_3(+UV); (b) The difference (aged minus fresh) of the average organic spectra of incense burning particles at 800 ppb O_3(+UV). The left axis and right axis are for negative spectra and positive spectra, respectively. (c) Number fraction of different categories in fresh, O_3-Dark-aged, and O_3-UV-aged particles.

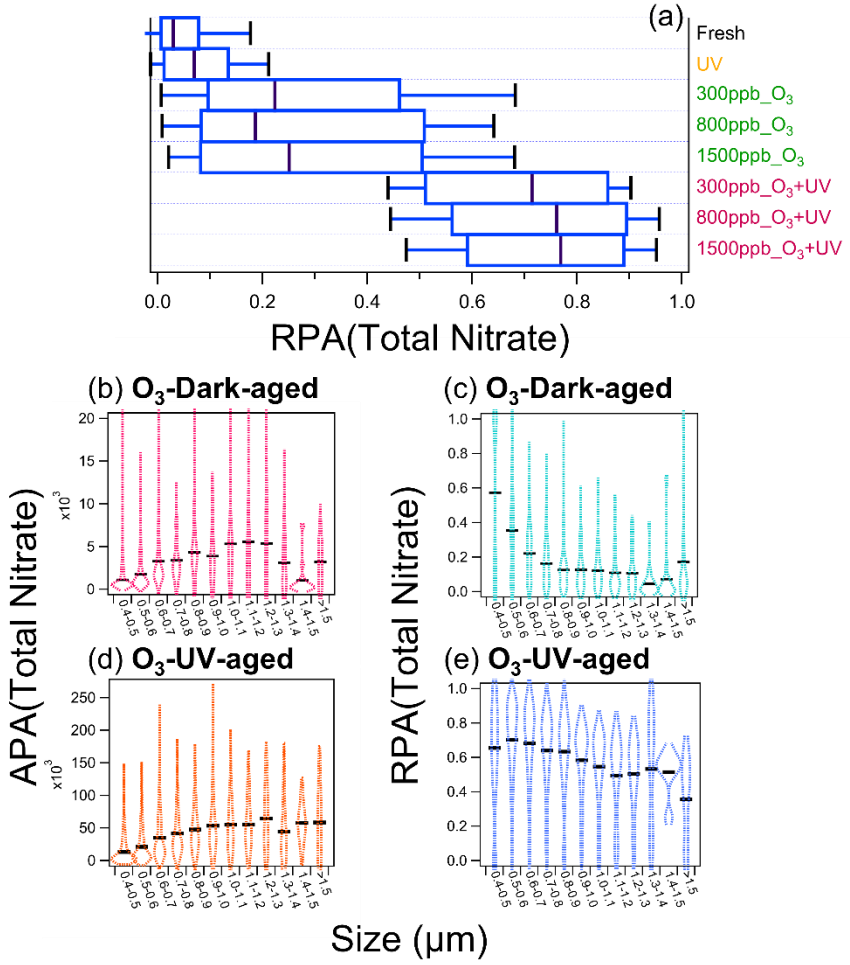

Figure 2. (a) The whisker-box plot of total nitrate RPA of fresh and aged particles. The violin plots of (b, d) APA and (c, e) RPA of total nitrate in O_3- and O_3-UV-aged particles as a function of size (unit: μm) of particles aged at 1500 ppb O_3 (+ UV). The medians are shown as the lines, and the kernel densities represent the probability density of the data at different values.

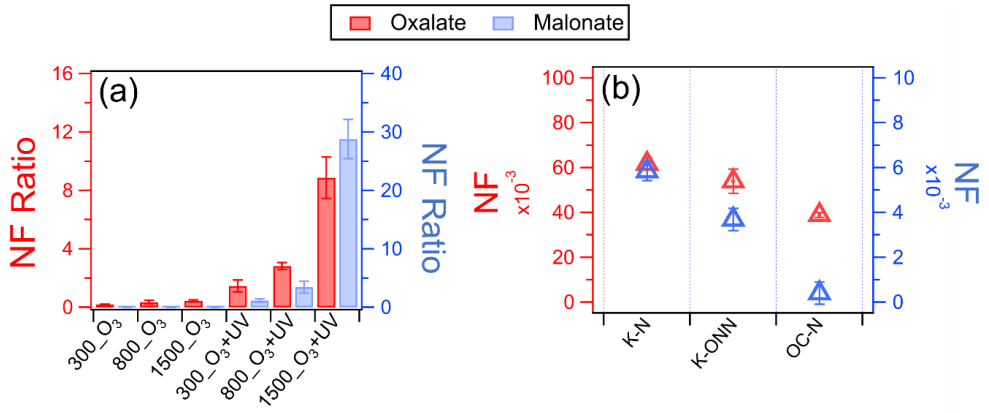

Figure 3. (a) The NF ratios of oxalate and malonate under different conditions. 300_O_3 denotes aging at 300 ppb O_3; (b) The NF of oxalate (left axis) and malonate (right axis) in different categories of aged particles.

Data availability. The supplement provides additional figures and tables.

Competing interests. The contact author has declared that neither they nor their co-authors have any competing interests.

Financial support.

Acknowledgment. We gratefully acknowledge the support from the Key-Area Research and Development Program of Guangdong Province (2020B1111360001), the Hong Kong Research Grants Council (No.11304121, R1016-20F), the National Natural Science Foundation of China (No. 42275104, 41905122).

References

Akagi, S. K., Yokelson, R. J., Wiedinmyer, C., Alvarado, M. J., Reid, J. S., Karl, T., Crounse, J. D., and Wennberg, P. O.: Emission factors for open and domestic biomass burning for use in atmospheric models, Atmos. Chem. Phys., 11, 4039-4072, 10.5194/acp-11-4039-2011, 2011.

Bi, X., Zhang, G., Li, L., Wang, X., Li, M., Sheng, G., Fu, J., and Zhou, Z.: Mixing state of biomass burning particles by single particle aerosol mass spectrometer in the urban area of PRD, China, Atmospheric Environment, 45, 3447-3453, https://doi.org/10.1016/j.atmosenv.2011.03.034, 2011.

Bootdee, S., Chantara, S., and Prapamontol, T.: Determination of PM2.5 and polycyclic aromatic hydrocarbons from incense burning emission at shrine for health risk assessment, Atmospheric Pollution Research, 7, 680-689, https://doi.org/10.1016/j.apr.2016.03.002, 2016.

Carrico, C. M., Petters, M. D., Kreidenweis, S. M., Collett Jr., J. L., Engling, G., and Malm, W. C.: Aerosol hygroscopicity and cloud droplet activation of extracts of filters from biomass burning experiments, Journal of Geophysical Research: Atmospheres, 113, https://doi.org/10.1029/2007JD009274, 2008.

Chan, L. P. and Chan, C. K.: Enhanced Reactive Uptake of Nonanal by Acidic Aerosols in the Presence of Particle-Phase Organics, Aerosol Science and Technology, 45, 872-883, 10.1080/02786826.2011.567314, 2011.

Chan, L. P., Lee, A. K. Y., and Chan, C. K.: Gas−Particle Partitioning of Alcohol Vapors on Organic Aerosols, Environmental Science & Technology, 44, 257-262, 10.1021/es9018018, 2010.

Chan, M. N., Choi, M. Y., Ng, N. L., and Chan, C. K.: Hygroscopicity of Water-Soluble Organic Compounds in Atmospheric Aerosols: Amino Acids and Biomass Burning Derived Organic Species, Environmental Science & Technology, 39, 1555-1562, 10.1021/es049584l, 2005.

Chen, X., Hopke, P. K., and Carter, W. P.: Secondary organic aerosol from ozonolysis of biogenic volatile organic compounds: chamber studies of particle and reactive oxygen species formation, Environmental science & technology, 45, 276-282, 2011.

Chen, X., Wang, H., Lu, K., Li, C., Zhai, T., Tan, Z., Ma, X., Yang, X., Liu, Y., Chen, S., Dong, H., Li, X., Wu, Z., Hu, M., Zeng, L., and Zhang, Y.: Field Determination of Nitrate Formation Pathway in Winter Beijing, Environmental Science & Technology, 54, 9243-9253, 10.1021/acs.est.0c00972, 2020.

Cheng, C., Li, M., Chan, C. K., Tong, H., Chen, C., Chen, D., Wu, D., Li, L., Wu, C., and Cheng, P.: Mixing state of oxalic acid containing particles in the rural area of Pearl River Delta, China: implications for the formation mechanism of oxalic acid, Atmospheric Chemistry and Physics, 17, 9519-9533, 2017.

Chu, Y., Cheng, T. F., Gen, M., Chan, C. K., Lee, A. K., and Chan, M. N.: Effect of ozone concentration and relative humidity on the heterogeneous oxidation of linoleic acid particles by ozone: an insight into the interchangeability of ozone concentration and time, ACS Earth and Space Chemistry, 3, 779-788, 2019.

Chuang, H.-C., Jones, T., Chen, Y., Bell, J., Wenger, J., and BéruBé, K.: Characterisation of airborne particles and associated organic components produced from incense burning, Analytical and bioanalytical chemistry, 401, 3095-3102, 2011.

Dall'Osto, M., Beddows, D. C. S., Kinnersley, R. P., Harrison, R. M., Donovan, R. J., and Heal, M. R.: Characterization of individual airborne particles by using aerosol time-of-flight mass spectrometry at Mace Head, Ireland, Journal of Geophysical Research: Atmospheres, 109, https://doi.org/10.1029/2004JD004747, 2004.

Dall'Osto, M., Ovadnevaite, J., Ceburnis, D., Martin, D., Healy, R. M., O'Connor, I. P., Kourtchev, I., Sodeau, J. R., Wenger, J. C., and O'Dowd, C.: Characterization of urban aerosol in Cork city (Ireland) using aerosol mass spectrometry, Atmospheric Chemistry and Physics, 13, 4997-5015, 2013.

Denkenberger, K. A., Moffet, R. C., Holecek, J. C., Rebotier, T. P., and Prather, K. A.: Real-time, single-particle measurements of oligomers in aged ambient aerosol particles, Environmental Science & Technology, 41, 5439-5446, 2007.

Donaldson, D. J. and Vaida, V.: The Influence of Organic Films at the Air−Aqueous Boundary on Atmospheric Processes, Chemical Reviews, 106, 1445-1461, 10.1021/cr040367c, 2006.

Enami, S., Hoffmann, M. R., and Colussi, A.: Absorption of inhaled NO2, The Journal of Physical Chemistry B, 113, 7977-7981, 2009.

Finlayson-Pitts, B., Wingen, L., Sumner, A., Syomin, D., and Ramazan, K.: The heterogeneous hydrolysis of NO 2 in laboratory systems and in outdoor and indoor atmospheres: An integrated mechanism, Physical Chemistry Chemical Physics, 5, 223-242, 2003.

Finlayson-Pitts, B. J. and Pitts Jr, J. N.: Chemistry of the upper and lower atmosphere: theory, experiments, and applications, Elsevier1999.

Gen, M., Zhang, R., and Chan, C. K.: Nitrite/Nitrous Acid Generation from the Reaction of Nitrate and Fe(II) Promoted by Photolysis of Iron–Organic Complexes, Environmental Science & Technology, 55, 15715-15723, 10.1021/acs.est.1c05641, 2021.

Gen, M., Liang, Z., Zhang, R., Go Mabato, B. R., and Chan, C. K.: Particulate nitrate photolysis in the atmosphere, Environmental Science: Atmospheres, 10.1039/D1EA00087J, 2022.

Goel, A., Mundra, R., and Ola, D.: Examination of Particle Characteristics and Quantification of Emission Factors for Smoke Generated from a Popular Indian Incense Burnt in an Experimental Chamber, in: Indoor Environmental Quality, Springer, 77-84, 2020.

Guazzotti, S. A., Coffee, K. R., and Prather, K. A.: Continuous measurements of size-resolved particle chemistry during INDOEX-Intensive Field Phase 99, Journal of Geophysical Research: Atmospheres, 106, 28607-28627, https://doi.org/10.1029/2001JD900099, 2001.

Ho, S. S. H. and Yu, J. Z.: Concentrations of formaldehyde and other carbonyls in environments affected by incense burning, Journal of Environmental Monitoring, 4, 728-733, 10.1039/B200998F, 2002.

Hodshire, A. L., Akherati, A., Alvarado, M. J., Brown-Steiner, B., Jathar, S. H., Jimenez, J. L., Kreidenweis, S. M., Lonsdale, C. R., Onasch, T. B., and Ortega, A. M.: Aging effects on biomass burning aerosol mass and composition: A critical review of field and laboratory studies, Environmental science & technology, 53, 10007-10022, 2019.

Ji, X., Le Bihan, O., Ramalho, O., Mandin, C., D'Anna, B., Martinon, L., Nicolas, M., Bard, D., and Pairon, J.-C.: Characterization of particles emitted by incense burning in an experimental house, Indoor Air, 20, 147-158, https://doi.org/10.1111/j.1600-0668.2009.00634.x, 2010.

Kang, E., Root, M., Toohey, D., and Brune, W.: Introducing the concept of potential aerosol mass (PAM), Atmospheric Chemistry and Physics, 7, 5727-5744, 2007.

Khezri, B., Chan, Y. Y., Tiong, L. Y. D., and Webster, R. D.: Annual air pollution caused by the Hungry Ghost Festival, Environmental Science: Processes & Impacts, 17, 1578-1586, 10.1039/C5EM00312A, 2015.

Kroll, J. H., Ng, N. L., Murphy, S. M., Flagan, R. C., and Seinfeld, J. H.: Secondary organic aerosol formation from isoprene photooxidation, Environmental science & technology, 40, 1869-1877, 2006.

Kucinski, T. M., Dawson, J. N., and Freedman, M. A.: Size-Dependent Liquid–Liquid Phase Separation in Atmospherically Relevant Complex Systems, The Journal of Physical Chemistry Letters, 10, 6915-6920, 2019.

Kumar, N. K., Corbin, J. C., Bruns, E. A., Massabó, D., Slowik, J. G., Drinovec, L., Močnik, G., Prati, P., Vlachou, A., and Baltensperger, U.: Production of particulate brown carbon during atmospheric aging of residential wood-burning emissions, Atmospheric Chemistry and Physics, 18, 17843-17861, 2018.

Kuwata, M. and Lee, W.-C.: 1-octanol-water partitioning as a classifier of water soluble organic matters: Implication for solubility distribution, Aerosol Science and Technology, 51, 602-613, 10.1080/02786826.2017.1283004, 2017.

Lee, S.-C. and Wang, B.: Characteristics of emissions of air pollutants from burning of incense in a large environmental chamber, Atmospheric Environment, 38, 941-951, https://doi.org/10.1016/j.atmosenv.2003.11.002, 2004.

Li, L., Huang, Z., Dong, J., Li, M., Gao, W., Nian, H., Fu, Z., Zhang, G., Bi, X., Cheng, P., and Zhou, Z.: Real time bipolar time-of-flight mass spectrometer for analyzing single aerosol particles, International Journal of Mass Spectrometry, 303, 118-124, https://doi.org/10.1016/j.ijms.2011.01.017, 2011.

Li, W. and Hopke, P. K.: Initial Size Distributions and Hygroscopicity of Indoor Combustion Aerosol Particles, Aerosol Science and Technology, 19, 305-316, 10.1080/02786829308959638, 1993.

Li, Y. J., Yeung, J. W. T., Leung, T. P. I., Lau, A. P. S., and Chan, C. K.: Characterization of Organic Particles from Incense Burning Using an Aerodyne High-Resolution Time-of-Flight Aerosol Mass Spectrometer, Aerosol Science and Technology, 46, 654-665, 10.1080/02786826.2011.653017, 2012.

Liang, Z., Zhang, R., Gen, M., Chu, Y., and Chan, C. K.: Nitrate Photolysis in Mixed Sucrose–Nitrate–Sulfate Particles at Different Relative Humidities, The Journal of Physical Chemistry A, 125, 3739-3747, 10.1021/acs.jpca.1c00669, 2021.

Liang, Z., Zhou, L., Infante Cuevas, R. A., Li, X., Cheng, C., Li, M., Tang, R., Zhang, R., Lee, P. K. H., Lai, A. C. K., and Chan, C. K.: Sulfate Formation in Incense Burning Particles: A Single-Particle Mass Spectrometric Study, Environmental Science & Technology Letters, 9, 718-725, 10.1021/acs.estlett.2c00492, 2022.

Lin, T.-C., Yang, C.-R., and Chang, F.-H.: Burning characteristics and emission products related to metallic content in incense, Journal of hazardous materials, 140, 165-172, 2007.

Liu, T., Wang, Z., Huang, D. D., Wang, X., and Chan, C. K.: Significant Production of Secondary Organic Aerosol from Emissions of Heated Cooking Oils, Environmental Science & Technology Letters, 5, 32-37, 10.1021/acs.estlett.7b00530, 2018.

Liu, T., Zhou, L., Liu, Q., Lee, B. P., Yao, D., Lu, H., Lyu, X., Guo, H., and Chan, C. K.: Secondary Organic Aerosol Formation from Urban Roadside Air in Hong Kong, Environmental Science & Technology, 53, 3001-3009, 10.1021/acs.est.8b06587, 2019.

Lu, K., Fuchs, H., Hofzumahaus, A., Tan, Z., Wang, H., Zhang, L., Schmitt, S. H., Rohrer, F., Bohn, B., Broch, S., Dong, H., Gkatzelis, G. I., Hohaus, T., Holland, F., Li, X., Liu, Y., Liu, Y., Ma, X., Novelli, A., Schlag, P., Shao, M., Wu, Y., Wu, Z., Zeng, L., Hu, M., Kiendler-Scharr, A., Wahner, A., and Zhang, Y.: Fast Photochemistry in Wintertime Haze: Consequences for Pollution Mitigation Strategies, Environ Sci Technol, 53, 10676-10684, 10.1021/acs.est.9b02422, 2019.

Luo, J., Zhang, J., Huang, X., Liu, Q., Luo, B., Zhang, W., Rao, Z., and Yu, Y.: Characteristics, evolution, and regional differences of biomass burning particles in the Sichuan Basin, China, Journal of Environmental Sciences, 89, 35-46, https://doi.org/10.1016/j.jes.2019.09.015, 2020.

Lyu, X., Huo, Y., Yang, J., Yao, D., Li, K., Lu, H., Zeren, Y., and Guo, H.: Real-time molecular characterization of air pollutants in a Hong Kong residence: Implication of indoor source emissions and heterogeneous chemistry, Indoor Air, 31, 1340-1352, https://doi.org/10.1111/ina.12826, 2021.

Manoukian, A., Quivet, E., Temime-Roussel, B., Nicolas, M., Maupetit, F., and Wortham, H.: Emission characteristics of air pollutants from incense and candle burning in indoor atmospheres, Environmental Science and Pollution Research, 20, 4659-4670, 10.1007/s11356-012-1394-y, 2013.

Mao, J., Ren, X., Brune, W., Olson, J., Crawford, J., Fried, A., Huey, L., Cohen, R., Heikes, B., and Singh, H.: Airborne measurement of OH reactivity during INTEX-B, Atmospheric Chemistry and Physics, 9, 163-173, 2009.

McFall, A. S., Johnson, A. W., and Anastasio, C.: Air–water partitioning of biomass-burning phenols and the effects of temperature and salinity, Environmental Science & Technology, 54, 3823-3830, 2020.

Neubauer, K. R., Johnston, M. V., and Wexler, A. S.: Humidity effects on the mass spectra of single aerosol particles, Atmospheric Environment, 32, 2521-2529, 1998.

Ng, N. L., Brown, S. S., Archibald, A. T., Atlas, E., Cohen, R. C., Crowley, J. N., Day, D. A., Donahue, N. M., Fry, J. L., and Fuchs, H.: Nitrate radicals and biogenic volatile organic compounds: oxidation, mechanisms, and organic aerosol, Atmospheric chemistry and physics, 17, 2103-2162, 2017.

Passig, J., Schade, J., Irsig, R., Kröger-Badge, T., Czech, H., Adam, T., Fallgren, H., Moldanova, J., Sklorz, M., and Streibel, T.: Single-particle characterization of polycyclic aromatic hydrocarbons in background air in northern Europe, Atmospheric Chemistry and Physics, 22, 1495-1514, 2022.

Peng, C. and Chan, C. K.: The water cycles of water-soluble organic salts of atmospheric importance, Atmospheric Environment, 35, 1183-1192, 2001.

Peng, X., Liu, X., Shi, X., Shi, G., Li, M., Liu, J., Huangfu, Y., Xu, H., Ma, R., Wang, W., and Feng, Y.: Source apportionment using receptor model based on aerosol mass spectra and 1 h resolution chemical dataset in Tianjin, China, Atmospheric Environment, 198, 387-397, https://doi.org/10.1016/j.atmosenv.2018.11.018, 2019.

Phares, D. J., Rhoads, K. P., Wexler, A. S., Kane, D. B., and Johnston, M. V.: Application of the ART-2a algorithm to laser ablation aerosol mass spectrometry of particle standards, Analytical Chemistry, 73, 2338-2344, 2001.

Qin, X. and Prather, K. A.: Impact of biomass emissions on particle chemistry during the California Regional Particulate Air Quality Study, International Journal of Mass Spectrometry, 258, 142-150, https://doi.org/10.1016/j.ijms.2006.09.004, 2006.

Ramazan, K., Wingen, L. M., Miller, Y., Chaban, G. M., Gerber, R. B., Xantheas, S. S., and Finlayson-Pitts, B. J.: New experimental and theoretical approach to the heterogeneous hydrolysis of NO2: Key role of molecular nitric acid and its complexes, The Journal of Physical Chemistry A, 110, 6886-6897, 2006.

Rissler, J., Vestin, A., Swietlicki, E., Fisch, G., Zhou, J., Artaxo, P., and Andreae, M. O.: Size distribution and hygroscopic properties of aerosol particles from dry-season biomass burning in Amazonia, Atmos. Chem. Phys., 6, 471-491, 10.5194/acp-6-471-2006, 2006.

Rudich, Y., Donahue, N. M., and Mentel, T. F.: Aging of organic aerosol: Bridging the gap between laboratory and field studies, Annu. Rev. Phys. Chem., 58, 321-352, 2007.

Schilling, J. B.: Extraction of semivolatile organic compounds from high-efficiency particulate air (HEPA) filters by supercritical carbon dioxide, Argonne National Lab., Analytical Chemistry Lab., IL (United States), 1997.

Schurman, M. I., Kim, J. Y., Cheung, H. H., and Chan, C. K.: Atmospheric particle composition-hygroscopic growth measurements using an in-series hybrid tandem differential mobility analyzer and aerosol mass spectrometer, Aerosol Science and Technology, 51, 694-703, 2017.

See, S. W. and Balasubramanian, R.: Characterization of fine particle emissions from incense burning, Building and Environment, 46, 1074-1080, https://doi.org/10.1016/j.buildenv.2010.11.006, 2011.

Seinfeld, J. and Pandis, S.: Atmospheric chemistry and physics. 1997, New York, 2008.

Sharma, V. K. and Graham, N. J. D.: Oxidation of Amino Acids, Peptides and Proteins by Ozone: A Review, Ozone: Science & Engineering, 32, 81-90, 10.1080/01919510903510507, 2010.

Sidibe, A., Sakamoto, Y., Murano, K., Sato, K., Yuba, A., Futami, M., Koita, O. A., Traore, I., and Kajii, Y.: Chemical Characterization and Health Risk Assessment of Particulate Matter from Household Activities in Bamako, Mali, Western Sub-Saharan Africa, Atmosphere, 13, 1290, 2022.

Silva, P. J. and Prather, K. A.: Interpretation of Mass Spectra from Organic Compounds in Aerosol Time-of-Flight Mass Spectrometry, Analytical Chemistry, 72, 3553-3562, 10.1021/ac9910132, 2000.

Silva, P. J., Liu, D.-Y., Noble, C. A., and Prather, K. A.: Size and Chemical Characterization of Individual Particles Resulting from Biomass Burning of Local Southern California Species, Environmental Science & Technology, 33, 3068-3076, 10.1021/es980544p, 1999.

Slade, J. H. and Knopf, D. A.: Multiphase OH oxidation kinetics of organic aerosol: The role of particle phase state and relative humidity, Geophysical Research Letters, 41, 5297-5306, 2014.

Spencer, M. T. and Prather, K. A.: Using ATOFMS to determine OC/EC mass fractions in particles, Aerosol Science and Technology, 40, 585-594, 2006.

Sullivan, R. C. and Prather, K. A.: Investigations of the diurnal cycle and mixing state of oxalic acid in individual particles in Asian aerosol outflow, Environmental Science Technology, 41, 8062-8069, 2007.

Taiwo, A. M., Harrison, R. M., Beddows, D. C., and Shi, Z.: Source apportionment of single particles sampled at the industrially polluted town of Port Talbot, United Kingdom by ATOFMS, Atmospheric Environment, 97, 155-165, 2014.

Volkamer, R., Jimenez, J. L., San Martini, F., Dzepina, K., Zhang, Q., Salcedo, D., Molina, L. T., Worsnop, D. R., and Molina, M. J.: Secondary organic aerosol formation from anthropogenic air pollution: Rapid and higher than expected, Geophysical Research Letters, 33, 2006.

Wang, B., Lee, S. C., and Ho, K. F.: Chemical composition of fine particles from incense burning in a large environmental chamber, Atmospheric Environment, 40, 7858-7868, https://doi.org/10.1016/j.atmosenv.2006.07.041, 2006.

Whiteaker, J. R., Suess, D. T., and Prather, K. A.: Effects of Meteorological Conditions on Aerosol Composition and Mixing State in Bakersfield, CA, Environmental Science & Technology, 36, 2345-2353, 10.1021/es011381z, 2002.

Xia, N., Du, E., Guo, Z., and de Vries, W.: The diurnal cycle of summer tropospheric ozone concentrations across Chinese cities: Spatial patterns and main drivers, Environmental Pollution, 286, 117547, https://doi.org/10.1016/j.envpol.2021.117547, 2021.

Xiao, H. W., Zhu, R. G., Pan, Y. Y., Guo, W., Zheng, N. J., Liu, Y. H., Liu, C., Zhang, Z. Y., Wu, J. F., and Kang, C. A.: Differentiation between nitrate aerosol formation pathways in a southeast Chinese city by dual isotope and modeling studies, Journal of Geophysical Research: Atmospheres, 125, e2020JD032604, 2020.

Yabushita, A., Enami, S., Sakamoto, Y., Kawasaki, M., Hoffmann, M., and Colussi, A.: Anion-catalyzed dissolution of NO2 on aqueous microdroplets, The Journal of Physical Chemistry A, 113, 4844-4848, 2009.

Yao, X., Fang, M., and Chan, C. K.: Size distributions and formation of dicarboxylic acids in atmospheric particles, Atmospheric Environment, 36, 2099-2107, 2002.

Yao, Y., Xie, Y., Zhao, B., Zhou, L., Shi, Y., Wang, Y., Sheng, Y., Zhao, H., Sun, J., and Cao, H.: N-dependent ozonation efficiency over nitrogen-containing heterocyclic contaminants: A combined density functional theory study on reaction kinetics and degradation pathways, Chemical Engineering Journal, 382, 122708, https://doi.org/10.1016/j.cej.2019.122708, 2020.

Ye, C., Chen, R., and Chen, M.: The impacts of Chinese Nian culture on air pollution, Journal of Cleaner Production, 112, 1740-1745, 2016.

Zaveri, R. A., Shilling, J. E., Zelenyuk, A., Liu, J., Bell, D. M., D'Ambro, E. L., Gaston, C. J., Thornton, J. A., Laskin, A., and Lin, P.: Growth kinetics and size distribution dynamics of viscous secondary organic aerosol, Environmental science & technology, 52, 1191-1199, 2018.

Zhai, J., Wang, X., Li, J., Xu, T., Chen, H., Yang, X., and Chen, J.: Thermal desorption single particle mass spectrometry of ambient aerosol in Shanghai, Atmospheric Environment, 123, 407-414, 2015.

Zhang, G., Lian, X., Fu, Y., Lin, Q., Li, L., Song, W., Wang, Z., Tang, M., Chen, D., Bi, X., Wang, X., and Sheng, G.: High secondary formation of nitrogen-containing organics (NOCs) and its possible link to oxidized organics and ammonium, Atmos. Chem. Phys., 20, 1469-1481, 10.5194/acp-20-1469-2020, 2020.

Zhang, S., Wang, Z., Zhang, J., Guo, D., and Chen, Y.: Inhalable cigarette-burning particles: Size-resolved chemical composition and mixing state, Environmental Research, 202, 111790, 2021.

Zhang, X., Xu, J., Zhai, L., and Zhao, W.: Characterization of Aerosol Properties from the Burning Emissions of Typical Residential Fuels on the Tibetan Plateau, Environmental Science & Technology, 56, 14296-14305, 10.1021/acs.est.2c04211, 2022.

Zhang, Y., Zhang, X., Sun, J., Hu, G., Shen, X., Wang, Y., Wang, T., Wang, D., and Zhao, Y.: Chemical composition and mass size distribution of PM 1 at an elevated site in central east China, Atmospheric Chemistry and Physics, 14, 12237-12249, 2014.

Zhao, W., Hopke, P. K., and Prather, K. A.: Comparison of two cluster analysis methods using single particle mass spectra, Atmospheric Environment, 42, 881-892, https://doi.org/10.1016/j.atmosenv.2007.10.024, 2008.

Zhao, Z.-Y., Cao, F., Fan, M.-Y., Zhai, X.-Y., Yu, H.-R., Hong, Y., Ma, Y.-J., and Zhang, Y.-L.: Nitrate aerosol formation and source assessment in winter at different regions in Northeast China, Atmospheric Environment, 267, 118767, 2021.

Zhu, S., Li, L., Wang, S., Li, M., Liu, Y., Lu, X., Chen, H., Wang, L., Chen, J., Zhou, Z., Yang, X., and Wang, X.: Development of an automatic linear calibration method for high-resolution single-particle mass spectrometry: improved chemical species identification for atmospheric aerosols, Atmos. Meas. Tech., 13, 4111-4121, 10.5194/amt-13-4111-2020, 2020.

Zuend, A., Marcolli, C., Luo, B. P., and Peter, T.: A thermodynamic model of mixed organic-inorganic aerosols to predict activity coefficients, Atmos. Chem. Phys., 8, 4559-4593, 10.5194/acp-8-4559-2008, 2008.